Long term cortical plasticity in visual retinotopic areas in humans with silent retinal ganglion cell loss

Otília C. d'Almeida, Catarina Mateus, Aldina Reis, Manuela M. Grazina, Miguel Castelo-Branco

PII: S1053-8119(13)00526-0
DOI: doi: 10.1016/j.neuroimage.2013.05.032
Reference: YNIMG 10471

To appear in: *NeuroImage*

Accepted date: 5 May 2013

Long term cortical plasticity in visual retinotopic areas in humans with silent retinal ganglion cell loss

Otília C. d'Almeida[1], Catarina Mateus[1], Aldina Reis[1,2], Manuela M. Grazina[3,4] and Miguel Castelo-Branco[1,*]

[1]Visual Neuroscience Laboratory, IBILI, Faculty of Medicine, University of Coimbra, Portugal

[2]Coimbra University Hospital, Coimbra, Portugal

[3]Biochemistry Institute, Faculty of Medicine, University of Coimbra, Portugal

[4]Centre for Neuroscience and Cell Biology, University of Coimbra, Portugal

E-mail addresses:

oalmeida@fmed.uc.pt (O.C.d'Almeida)

mcbranco@fmed.uc.pt (M.Castelo-Branco)

*** Correspondence to:**

Miguel Castelo-Branco

Visual Neuroscience Laboratory, IBILI, Faculty of Medicine,

University of Coimbra, Azinhaga de Santa Comba

3000-548 Coimbra, Portugal

Phone: +351-239480200

Fax: +351-239480217

E-mail: mcbranco@fmed.uc.pt

ABSTRACT

Visual cortical plasticity induced by *overt* retinal lesions (scotomas) has remained a controversial phenomenon. Here we studied cortical plasticity in a *silent* model of retinal ganglion cell loss, documented by in vivo optical biopsy using coherence tomography. The cortical impact of non scotomatous subtle retinal ganglion cell functional and structural loss was investigated in carriers of the mitochondrial DNA 11778G>A mutation causing Leber's hereditary optic neuropathy. We used magnetic resonance imaging (MRI) to measure cortical thickness and fMRI to define retinotopic cortical visual areas V1, V2 and V3 in silent carriers and matched control groups.

Repeated measures analysis of variance revealed a surprising increase in cortical thickness in the younger carrier group (below 21 years of age). This effect dominated in extrastriate cortex, and notably V2. This form of structural plasticity suggests enhanced plastic developmental mechanisms in extrastriate retinotopic regions close to V1 and not receiving direct retinocortical input.

RUNNING TITLE

Cortical plasticity induced by silent visual loss

HIGHLIGHTS

- Unexpected increase in visual cortical thickness in early silent ganglion cell loss
- Retinotopically defined area V2 shows evidence for early compensatory plasticity
- Later in life plasticity migrates further to extrastriate V3 area

KEYWORDS

Cortical plasticity; visual loss; retinotopic visual areas; ganglion cells; development; mitochondrial gene mutations

ABBREVIATIONS

Retinal ganglion cell (RGC); Leber Hereditary Optic Neuropathy (LHON); lateral geniculate nucleus (LGN); primary visual cortex (V1); lesion projection zone (LPZ); cortical thickness (CT)

1 INTRODUCTION

It is known that the brain is able to optimize neural connectivity, in particular during critical periods (Eysel, 2009). Cortical plasticity is characterized by the modification of wiring of neuronal cortical networks in response to changes in visual experience, leading to structural and functional reorganization. Even though developmental plasticity is a well-established phenomenon, adult plasticity still is a very controversial issue. The ability of the cerebral cortex to adapt to changes in visual experience and mechanisms underlying compensation of loss of function are still highly debated (Wandell and Smirnakis, 2009). Nevertheless human studies have suggested that during the lifespan the cortex maintains the ability to structurally and functionally reorganize either to increased use or disuse due to lesions (Baseler et al., 2009; Bridge et al., 2008, 2010).

Animal model studies of artificially induced retinal lesions (for a review see Baseler et al., 2009) suggest that the cortex preserves a certain degree of plasticity and is capable of rewiring in response to loss of sensory inputs using the remaining intact portions of the retina. However, the mechanisms of visual plasticity induced by sustained silent loss of afferent retinal inputs in humans have hitherto not been studied.

We have addressed this issue by studying the silent stage of a human model of retinal ganglion cell (RGC) degeneration and death, Leber Hereditary Optic Neuropathy (LHON). LHON is an inherited genetic condition that may lead to loss of vision that becomes suddenly apparent after years of subtle neural loss. It is one of the most common types of hereditary optic atrophies with an estimated prevalence rate of approximately 1 in 30,000 (Man et al., 2003;

Newman and Biousse, 2004). This maternally inherited disorder caused by point mutations in the mitochondrial DNA (Kirkman et al., 2009b) is characterized by optic nerve atrophy and reduced retinocortical processing. After clinical onset it leads to bilateral visual impairment with dominant loss of central vision (Kirkman et al., 2009a).

Retinocortical information flow is routed from the optic nerve to the lateral geniculate nucleus (LGN) and then dominantly to the primary striate visual cortex (V1). Visual information is then redistributed to extrastriate V2, V3 and higher visual areas (Felleman and Van Essen, 1991). Retinal degeneration does therefore directly deprive V1 from receiving sensory information.

The main aim of this study was to elucidate the structural impact of silent early stage deprivation. An important question was whether indirectly deprived visual extrastriate regions would be affected, or instead reorganize.

It is worth emphasizing that we did not study here overt or late stage clinical cases, where lack of direct input might lead to manifest cortical atrophy and grey matter thinning. Such overt loss might explain putative cortical atrophy in lesion projection zones (LPZ) of clinically established retinal lesions. Accordingly, a study comparing grey matter density in visual cortex of foveal (age-related macular degeneration) and peripheral (open-angle glaucoma) retinal lesion models using Voxel Based Morphometry revealed reduction in grey matter density in the respective LPZs in the calcarine sulcus (Boucard et al., 2009). This shows that overt lesions as expressed by visual field scotomata may lead to retinotopic-specific structural loss in the visual cortex.

Our study focuses on the impact of widespread but clinically silent early afferent degeneration on primary striate and extrastriate cortex reorganization. We

computed cortical thickness (CT) maps in a pedigree of LHON individuals carrying the 11778G>A mitochondrial DNA mutation in functionally defined early visual areas V1, V2 and V3 in comparison with age-matched controls. Importantly, we expected plasticity to occur mainly during cortical development and to be reduced in adulthood due to decreased plasticity and progression of silent neurodegeneration. It was therefore important to set late developmental cutoffs defined by the onset of early adulthood. We found evidence for differential reorganization in this age-dependent model of silently progressive loss.

2 MATERIAL AND METHODS

2.1 Subjects

We have tested 15 asymptomatic LHON carriers (7 men, 8 women; mean age=29.3±13.50 [SD] years; age range, 8-47 years) (Table 1) that belong to a single homogeneous pedigree of confirmed presence of the mitochondrial DNA 11778G>A mutation (Grazina et al., 2007). Participants from the LHON group were submitted to MRI acquisition and data were compared to subjects from an age-matched control group (n=15 participants; 11 men, 4 women; mean age=26.2±11.45 [SD] years; age range, 7-44 years).

All participants were submitted to a complete ophthalmological examination, including best-corrected visual acuity obtained with Snellen chart, ocular tension (Goldmann applanation tonometer, slit lamp biomicroscopy and fundus examination (Goldmann lens)). Control subjects were required to have good visual acuity and not to have any visual field defect (as defined by normative data). Our participants from the LHON carrier group had normal ocular

examination, with normal visual acuity and no fundus changes. Visual functional evaluation (see Table 1) showed subclinical impairment in chromatic contrast sensitivity for all color axes (Cambridge Colour Test -Cambridge Research Systems, Rochester, UK: Protan: p=0.002; Deutan: p=0.006; Tritan: p=0.007). Subtle changes in the visual field sensitivity, in spite of the absence of scotomas (Octopus - Haag-Streit AG, Germany), with impact in the global threshold parameters (mean±SD, mean defect (MD): 3.76±2.10 dB); and loss of variance (LV): 8.36±7.31 dB^2), could also be found (Table 1). The normal range considered for MD and LV are ±2 dB and < 6 dB^2, respectively. Structural evaluation of the neural retina was performed using optical coherence tomography, a form of optical biopsy (Stratus OCT3 - Humphrey, Carl Zeiss Meditec, Dublin, CA, USA, axial resolution ~ 10 µm, for details see below). Exclusion criteria were established pseudophakic and aphakic eyes, significant media opacities, other retinal diseases, high ammetropy (sphere>+4D; cylinder>+2D) and other neuro–ophthalmologic pathology, besides LHON. The study followed the tenets of the Declaration of Helsinki and was approved by our Institutional Review Board. Informed consent was obtained from each participant and after research procedures had been fully explained.

Insert TABLE 1 about here

2.2 Retinal Imaging

Optical Coherence Tomography (Stratus OCT3, Humphrey, Carl Zeiss Inst., CA, USA) provides a cross-sectional tomography of retinal tissue in real time, based on optical interferometry, using infra-red (843 nm), low coherence light.

Cross-sectional images of retinal anatomy were thus obtained, with an axial resolution of ≤10 µm. Retinal thickness was computed as a 9 region bidimensional interpolated thickness map, with a central circle of 1 mm diameter and 2 outer circles with diameter of 3 and 6 mm (Fig. 1).

Insert FIGURE 1 about here

2.3 Stimuli and task design

2.3.1 *Retinotopic mapping*

Early visual areas are retinotopically arranged in the human visual cortex and mirror/nonmirror representations of adjacent areas of the visual field correspond to the turning points in horizontal and vertical meridians. Visual field mapping fMRI data were acquired using visual stimuli encoding polar coordinates. We used the standard travelling-wave method (phase-encoded retinotopy) (Engel et al., 1994; Sereno et al., 1995). Presented stimuli were: (i) polar angle encoding stimuli (Fig. 2B) comprised by a rotating (anticlockwise) black and white checkered wedge flickering at 8 Hz (48 s full cycle, 4 cycles/scan, three scans per subject) and (ii) an eccentricity mapping paradigm (Fig. 2C), using an expanding black and white checkered annulus flickering at 8 Hz (48s each full expansion, 4 expansions/scan, one scan per subject), while the subject was instructed to fix an orange-colored central point. The stimuli spanned 23º*23º of visual angle (diameter). This method allowed the mapping of the visual field angular position and eccentricity in relation to the centre of the gaze (see below details of fMRI analysis).

Insert FIGURE 2 about here

2.4 Data acquisition

High resolution MRI data was acquired in a 3T scanner (Siemens Magnetom TrioTim 3T Erlangen, Germany) at the Portuguese Brain Imaging Network, with a 12 channel head coil. The MRI acquisition protocol for each participant was: (i) two 9-minute long T1-weighted (T1w) three-dimensional Magnetization Prepared Rapid Acquisition Gradient Echo (MPRAGE) sequences, repetition time (TR) 2.3 s, echo time (TE) 2.98 ms, flip angle (FA) 9º, field of view (FoV) 256x256 mm^2, yielding 160 slices with 1x1x1 mm^3 voxel size; (ii) four functional runs (three polar angle and one eccentricity stimuli) using single shot echo planar imaging (EPI) acquired in the axial plane orthogonal to the anterior commissure covering the occipital, temporal and frontal cortices, TR 2 s, TE 39 ms with a 128x128 imaging matrix, interslice time 76 ms, FA 90º, FOV 256x256 mm^2, yielding 26 slices with 2x2x2 mm^3 voxel size.

2.5 Data Analysis

All image processing, cortical thickness and retinotopic mapping was performed with BrainVoyager QX 2.2 (Brain Innovation, Maastricht, The Netherlands) (Fig. 2). Thickness values of each visual area were extracted with BVQX toolbox for MATLAB (R2008a, v.7.6.0, The MathWorks, USA). For details on statistical analysis see below.

2.5.1 *Anatomical Image processing*

Structural data processing was as described in Geuze et al. (2008). Anatomical data were converted from DICOM to Brainvoyager's internal data format. To reduce the intensity variations caused by the magnetic field and RF-field inhomogeneities, we applied a bias-field mask (Dale et al., 1999). The two high-resolution T1w anatomical images were averaged, to improve the signal-to-noise ratio. To clean the data we applied a "brain peeling" tool (Goebel et al., 2006) to automatically "skull-strip" and remove the extra-cerebral voxels. The anatomical volumes were re-oriented in relation to the anterior and posterior commissure plane (AC-PC) and transformed to Talairach (TAL) (Talairach and Tournoux, 1988) coordinate system. Thereon, cortex was segmented using automatic segmentation routines (Kriegeskorte and Goebel, 2001) to create mesh representations of each hemisphere. To visualize all cortical activity, from gyri to sulci, we morphed each reconstructed hemisphere, and inflated it. Thereafter, we drew manually a cut along the calcarine fissure and flattened each hemisphere (Fischl et al., 1999). Meshes were inflated and flattened for surface maps projection (Fig. 2).

2.5.2 *Cortical Thickness Assessment*

To allow an accurate segmentation of WM-GM and GM-CSF boundary and since 0.5 mm resolution is better suited to measure cortical thickness by the Laplace method (Jones et al., 2000), TAL anatomical data were converted to high-resolution 0.5 x 0.5 x 0.5 mm iso-voxels using sinc interpolation iso-voxels (Geuze et al., 2008). Subcortical structures and the ventricles were filled as white matter (WM). To sort white from grey matter (GM) voxels, we used an adaptive region growing step based on locally computed intensity histograms

and calculated gradient information. Thereafter, the GM-cerebrospinal fluid (CSF) border was also segmented with a dilation process starting at the WM-GM border. Finally both borders were polished. The final step allowed for definition of two boundaries translated into two different intensity values, defining the WM-GM and GM-CSF boundaries.The measurement of cortical thickness can lead to miscalculations, in both manual or automatical approaches (Fischl and Dale, 2000), due to the highly convoluted structure of the cortical surface. To reduce the error probability we used an automatic algorithm that applies the second-order partial differential Laplace's equation (Jones et al., 2000). The solution of Laplace's equation is equivalent to smooth transition of intensities between the two boundaries. The program calculates a gradient value for each voxel. Starting at each boundary voxel the algorithm performs continuously small steps along the gradient's direction at each point. The sum of the small step sizes performed between the two borders gives the cortical thickness values (Geuze et al., 2008). After the computation, a cortical thickness map was superimposed in the volumetric (VMR) data file, and then interpolated into the inflated cortical meshes (Fig. 2A).

2.5.3 Functional Image Processing

The fMRI datasets were pre-processed as follows: slice scan time correction, cubic-spline interpolation, small 3D interscan head motion correction with sinc estimation and interpolation, space domain 3D spatial smoothing (Gaussian filter of 2mm) and temporal filtering (high pass, 2 cycles per run).

Polar angle maps were obtained from the average of three runs. Both polar angle and eccentricity maps were created based on linear regression analysis

(HRF=5s) and projected onto the TAL anatomical surfaces of each subject. The cross-correlation was calculated for each run, as a function of the time lag (in TR units, 2 seconds per lag). Lag values at each voxel were encoded in pseudocolors, voxels were included into the statistical map if $r > 0.25$, $p < 0.05$.

2.5.4 *Retinotopic mapping*

Sereno et al. (1994) described an accurate method for delineating early visual areas, using information both from polar angle (Fig. 3A) and eccentricity (Fig. 3B) mapping experiments. The eccentricity and polar angle gradients define field sign maps that reflect the mirrored representation of visual areas. Hence, we obtained two-color code mapping that established the lateral boundaries of the cortical visual areas (Fig. 3C). Retinotopic areas V1, V2 and V3 were manually defined over flattened meshes for each subject in each hemisphere using Brainvoyager's surface drawing tools (Fig. 3D). Obtained regions-of-interest (ROIs) were used as "masks" to the analysis of regional cortical thickness.

Insert FIGURE 3 about here

2.6 Statistical Analysis

Each hemisphere was considered individually and a region-of-interest approach was applied. Using a Matlab (MATLAB R2008a, The Mathworks, USA) interface, ROIs were superimposed in the CT maps and the mean values of thickness for each area were calculated. To prevent outlier biases, an outlier

removal criterion was considered. This approach consisted in the recalculation of the mean excluding the values deviating more than 3 standard deviations (SD) of the mean.

All statistical analyses were performed with IBM SPSS Statistics 20 for Windows (version 20, IBM Corp, Armonk, NY, USA). Parametric tests were performed subsequent to prior verification of normality assumption (non-parametric Kolmogorov-Smirnov test, $p > 0.05$). The statistical analysis was based on the General Linear Model multivariate analysis of variance (MANOVA) for homologous ROIs between group comparisons. Further analysis were done in younger and older age cohorts separately (using a developmental cut-off criterion of 21 years, see Introduction). We also calculated Cohen's d from F-tests to evaluate the effect size of the MANOVA statistical results. In addition, to analyze the spatial specificity of effects we performed between group independent samples t-tests for two anatomically-defined non-visual control regions, precentral and postcentral gyrus.

To analyze ROIs thickness differences within each group, we used parametric GLM Repeated Measures ANCOVA (rmANCOVA), setting age as a metric covariate. We also performed a rmANCOVA adding also gender as a putative confound. When the data did not meet assumptions of sphericity, we used the epsilon value to choose the type of correction applied: the Huynh-Feldt (for $\varepsilon > 0.75$) or the Greenhouse–Geisser (for $\varepsilon < 0.75$). Repeated measures ANOVA was performed to assess group differences between visual areas cortical thickness in each of the two age subgroups.

Multiple comparisons *post-hoc* tests were based on the Bonferroni correction. We also checked for correlations between ROIs and between age and visual areas with Pearson's correlation analyses.

Moreover, we performed correlation analysis between retinal thickness measures across eccentricity rings (using OCT Stratus) and thickness of cortical visual areas. All statistical data is presented as the mean ± SEM (standard error of the mean). Two-tailed hypothesis testing was performed at a 0.05 significance level.

3 RESULTS

Mean cortical thickness was calculated as the average of all vertices inside each functionally defined low-level visual area V1, V2, and V3 (n=30 hemispheres for each group, see Fig. 2, 3 and Material and Methods section). As in this genetic condition RGCs are specifically affected, we measured the integrity of the neural retina. We found decreased thickness of the neural retina in the central ring ($p<0.05$), when compared with controls (Fig. 1 and Table 1), showing the impact of silent RGC loss.

3.1 Cortical thickness in retinotopically defined areas

3.1.1 LHON carriers, bearing silent visual loss, have thicker extrastriate visual cortical areas as compared to controls

Overall higher values of cortical thickness were observed for the LHON group (Fig. 4). Multivariate analysis MANOVA for visual areas V1, V2 and V3, showed a statistically significant difference between groups for extrastriate areas V2 and V3 (V2: $F(1,58)=7.309$, $p=0.009$, Cohen's $d=0.71$; V3: $F(1,58)=5.539$, $p=0.022$,

Cohen's d=0.62). **Between group comparisons of cortical thickness within the precentral (t(58)=0.860) and the postcentral gyrus (t(58)=1.177) showed no differences (n.s.), which suggests that we have indeed found a specific pattern of reorganization.**

Insert FIGURE 4 about here

To specifically compare ROIs cortical thickness within each group, we performed rmANCOVA with visual area (V1, V2 and V3) cortical thickness as within-subjects factor for each group (LHON and control) separately, and adding age as a possible confound.

As expected the control group showed no differences in mean cortical thickness across visual areas. However, we found that cortical thickness differed significantly across visual areas in LHON carriers (Huynh-Feldt correction, $F(1.746,48.885)=6.059$, $p=0.006$), suggesting differential reorganization processes.

Post hoc tests using the Bonferroni correction, to identify the sources of the main effect, suggested that increased cortical thickness in LHON is due to the difference in thickness between both extrastriate areas V2 and V3 and V1 (V1-V2, $p=0.061$; V1-V3, $p=0.035$) with no evidence for differences between extrastriate regions (ns).

Even though the LHON carrier group was balanced in gender, the control group was not. Therefore we performed a Repeated Measures ANOVA, using group as between subjects factor, each ROI as within subjects factor and both gender

and age as covariates. We found that there was neither an interaction between visual area cortical thickness with gender nor a gender effect (n.s).

3.1.2 *Group differences in cortical thickness across visual areas prior to and after the end developmental maturation*

In rmANCOVA, setting age as covariate, both within control and LHON carrier groups a main effect of age was found ($F(1,28)=7.743$, $p=0.010$; $F(1,28)=24.060$, $p<0.001$, respectively). We also have found in LHON a significant interaction between the effects of visual area mean thickness and age (Huynh-Feldt correction, $F(1.746,48.885)=3.371$, $p=0.049$), suggesting that a neural plasticity profile consistent with the differential changes in striate vs. extrastriate regions in the group with silent retinal loss.

For this reason, and to probe early vs. post developmental (early adulthood) effects, we have divided each group into two subgroups using the developmental cut-off criterium of 21 years of age ("≤21" and ">21" subgroups). By splitting each group into "≤21" and ">21" subgroups, we could then perform a group comparison accross visual areas between using (M)ANOVA. We confirmed that mean cortical thickness in the LHON carrier group was, on average, higher than in the control group both under and over 21 years. Fig. 5 shows that this difference is mainly caused by differences in V2 thickness across groups in younger subjects and in V3 in older subjects, suggesting that the differential role of extrastriate areas changes across age. ANOVA analysis showed indeed that there was a generally significant difference in cortical thickness between control and LHON carrier groups, in particular for V2 ($F(1,22)=8.312$, $p=0.009$, Cohen's $d=1.23$) below 21 years old, and in V3

(F(1,34)=8.934, p=0.005, Cohen's d=1.03) in participants over 21 years old. In the two age subgroups we performed a rmANOVA analysis with V1, V2 and V3 (visual area cortical thickness) as the within-subjects factors and group (LHON and control) as between-subjects factor. We confirmed a significant effect of visual area specific to ≤21 subgroups (F(2,44)=3.288, p=0.047). The visual area effect in the younger age group can, as expected, be attributed mainly to the difference between visual areas thickness in the LHON carrier group (F(2,22)=5.606, P=0.011, rmANOVA for ≤21 LHON group), particularly between areas V1 and V2 (Bonferroni *post-hoc* analysis, p=0.053). These differences were, absent in the >21 subgroup. Fig. 6 shows examples of cortical thickness in a young LHON carrier and a control.

Insert FIGURE 5 about here

Insert FIGURE 6 about here

3.2 Regression of cortical thickness with age

Pearson correlation coefficients were computed to identify any potential associations between each individual's visual areas mean cortical thickness and also age in younger and older groups. We found interesting correlational patterns between visual areal thickness and age for control and LHON groups, both under and over 21 years (see Table 2). A strong negative correlation was found in the ≤21y control group between V3 and age, and in the ≤21y LHON *carrier* group between both V2 and V3 and age. Areas within the control group showed no significant early correlation patterns (but only late – in adulthood), in contrast with the LHON group.

Correlation analysis between global (all lamina) retinal thickness measures across eccentricity rings and cortical thickness measures in LHON carrier group showed only strong significant positive correlations between the most peripheral ring, where the neural retina is still largely preserved, and extrastriate areas V2 (r=.582, p=.023) and V3 (r=.537, p=.039). **Retinal lamina analysis, separating fiber layers from neural cell body layers, using high resolution retinal imaging might be helpful in future studies to further elucidate the correlation patterns found in these patients.**

Insert TABLE 2 about here

4 DISCUSSION

We found that silent carriers of mitochondrial mutations affecting retinal ganglion cells (Carelli et al., 2007; Inglese et al., 2001) have profound changes in brain organization and plasticity, even when structural and functional neural loss is clinically silent and in the absence of scotomas.

Evidence for changed brain organization was expressed by increased cortical thickness that dominated in extrastriate areas throughout early visual development in LHON. This is to our knowledge, the first report describing positive plastic changes in cortical extrastriate regions in an asymptomatic condition leading to subcortical afferent loss.

It is possible that latent mitochondrial dysfunction leads to the here reported developmental plasticity. This interpretation is consistent with the knowledge that mitochondria play important roles in sculpting cytoarchitecture during development of the nervous system and that the location or properties of

mitochondria change in association with developmental processes (for a review see Mattson et al., 2008). This interpretation is also in line with well documented role of mitochondria in controlling brain plasticity (for a review see Mattson et al., 2008).

The fact that effect sizes of differences in thickness are larger in V2, which neighbors the region with direct afferent loss (V1) suggests that compensatory developmental plasticity is indeed a major mechanism underlying changes in thickness patterns across visual regions. Taken together, and since V1 suffers from impaired retinocortical input even in preclinical stages, these effects are consistent with a topological mechanism whereby neighboring area V2 shows increased compensatory thickness. This effect seems to be specific given that non visual areas (in precentral and postcentral gyrus regions) did not show changes.

Previous studies focused on plasticity related to visual scotomas or other acquired lesions (for a review see Wandell and Smirnakis, 2009). Our work addresses a very distinct form of plasticity because here we studied a preclinical carrier stage model of ganglion cell degeneration without visual symptoms in spite of the evidence for subtle psychophysical changes, and absence of scotomas.

Other studies have analyzed the structural impact of long-term cortical deprivation and visual loss as assessed by the expected grey matter density changes in the correspondent visual representations (Boucard et al., 2009). These identified losses are to be expected from late stage clinically affected adults in whom neural degeneration and visual symptoms dominate over plasticity which is rather limited at such stages. This was the case of previous

work using voxel-based morphometry (VBM) reporting brain degeneration in largely impaired patients with clinically installed LHON, with reduced GM volume in putative (non retinotopically mapped) visual cortex, with damage in anterior visual pathways and in optic radiations (OR) (Barcella et al., 2010). In our study we addressed prelesional states of silent degeneration spanning developmental windows of available neural plasticity.

The long term period of brain adaptation that we could access largely exceeds the ones often available in experimental situations in which it becomes rather difficult to identify significant remapping or reorganization (Baseler et al., 2011). Accordingly, many studies cover a narrow age span, involve older age groups, and end stage disease. Consequently, neurodegeneration dominates and plastic reorganization mechanisms become barely noticeable (Bridge et al., 2010).

Our combination of retinotopic mapping with cortical thickness measures to identify differences in explicitly localized visual areas V1, V2 and V3 enabled interindividual matching and enhanced the power to detect plastic changes. These visual cortical areas do therefore seem to differently reorganize even in carriers of a mutation leading to abnormal physiology of retinal input cells. Since maturation of cerebral structures also involves the pruning of neuronal processes, lack of such pruning is also a potential explanation for the overall early increase in cortical thickness in LHON carriers (Low and Cheng, 2006; Tamnes et al., 2010). In our study, both LHON and control groups showed a pattern of age-dependent cortical thickness decrease which is consistent with previous studies (Salat et al., 2004). **Moreover, our correlation results are in**

agreement with the notion that higher level regions tend to mature later and have a different pattern in LHON and control subjects.

In any case, the most relevant finding in this study was the early increased thickness of extrastriate V2 (and into a smaller extent, V3) representations. Early visual information processing is mainly routed through V1 (receiving direct input from the LGN) and V2 (Felleman and Van Essen, 1991; Kaas et al., 2006). There is a strong functional relationship between V1 and V2 including feed-forward and feed-back projections (Sincich and Horton, 2005). The possibility that V2 can take over or compensate loss of function in V1 is also supported by brain damage data from Bridge et al. (2008).

As stated above our study goes beyond studies in humans or animal models with retinal lesion-induced lesions because in our model there is no overt lesion (scotoma) in the carrier state. The placement of retinal laser lesions in cats and monkeys, monocular or binocularly produces a lesion projection zone (LPZ) in V1. Neurons inside the LPZ gradually become responsive to stimuli presented to more peripheral, intact retinal locations (Baseler et al., 2009; Giannikopoulos and Eysel, 2006; Kaas et al., 1990). This plastic reorganization has significance but limited spatial extent, being restricted to few neighboring millimeters in the cortex and maybe mediated by local cortico-cortical connections (Calford et al., 2003; Darian-Smith and Gilbert, 1994). In spite of the differences between models, balance between growth and regressive factors are likely of equal importance (Kaas et al., 2006). Accordingly, it is possible that in LHON patients alternative pathways are formed, strengthened and/or recruited, to rescue the functionality that is more rapidly lost in V1. Age dependency of this type of effects (Giedd et al., 1999) suggests that neuroplasticity is dependent on

interaction between neurodevelopmental trajectories and neurodegenerative processes.

In sum, we found structural plastic reorganization, in a carrier state of disease model of RGC degeneration that is specific to developmental stages, in the absence of visual scotomas. The fact that extrastriate areas show a distinct pattern or reorganization, with specific thickening of V2/V3 in this silent model of afferent loss, may provide clues for the development of effective strategies for rehabilitation.

5 CONCLUSION

These results show that sensory deprivation in early and asymptomatic ganglion cell degeneration leads to differential regional-specific plasticity of regions of human visual cortex. These effects are age dependent, suggesting that early developmental plasticity causes increased thickness in extrastriate cortex. Such unexpected extrastriate structural plasticity overcomes the cortical atrophy expected from neurodegeneration in particular in striate cortex. The evidence of specific structural plasticity of extrastriate area V2 in this model of silent afferent loss reveals the presence of robust compensatory mechanisms with implications for rehabilitation approaches.

6 ACKNOWLEDGEMENTS

We do thank the LHON family, as well as all the control subjects that participated in this study. We also thank Carlos Ferreira and João Marques for help with MRI scanning and Pedro Guimarães for MatLab scripting. We do thank João Pratas for the technical assistance in mtDNA analysis. This work

was supported by the Portuguese Foundation for Science and Technology [grant numbers COMPETE, PTDC/SAU-NEU/68483/2006, PIC/IC/82986/2007, PTDC/SAU-ORG/118380, PEst – C/SAU/UI3282/2011 and individual fellowships SFRH/BD/64306/2009 to C.M., SFRH/BD/76013/2011 to O.A.].

7 REFERENCES

Barcella, V., Rocca, M.A., Bianchi-Marzoli, S., Milesi, J., Melzi, L., Falini, A., Pierro, L., and Filippi, M. (2010). Evidence for retrochiasmatic tissue loss in Leber's hereditary optic neuropathy. Hum. Brain Mapp. *31*, 1900–1906.

Baseler, H.A., Gouws, A., Haak, K.V., Racey, C., Crossland, M.D., Tufail, A., Rubin, G.S., Cornelissen, F.W., and Morland, A.B. (2011). Large-scale remapping of visual cortex is absent in adult humans with macular degeneration. Nat. Neurosci. *14*, 649–655.

Baseler, H.A., Gouws, A., and Morland, A.B. (2009). The Organization of the Visual Cortex in Patients with Scotomata Resulting from Lesions of the Central Retina. Neuroophthalmology *33*, 149–157.

Boucard, C.C., Hernowo, A.T., Maguire, R.P., Jansonius, N.M., Roerdink, J.B.T.M., Hooymans, J.M.M., and Cornelissen, F.W. (2009). Changes in cortical grey matter density associated with long-standing retinal visual field defects. Brain *132*, 1898–1906.

Bridge, H., Hicks, S.L., Xie, J., Okell, T.W., Mannan, S., Alexander, I., Cowey, A., and Kennard, C. (2010). Visual activation of extra-striate cortex in the absence of V1 activation. Neuropsychologia *48*, 4148–4154.

Bridge, H., Thomas, O., Jbabdi, S., and Cowey, A. (2008). Changes in connectivity after visual cortical brain damage underlie altered visual function. Brain *131*, 1433–1444.

Calford, M.B., Wright, L.L., Metha, A.B., and Taglianetti, V. (2003). Topographic plasticity in primary visual cortex is mediated by local corticocortical connections. J. Neurosci. *23*, 6434–6442.

Carelli, V., La Morgia, C., Iommarini, L., Carroccia, R., Mattiazzi, M., Sangiorgi, S., Farne', S., Maresca, A., Foscarini, B., Lanzi, L., et al. (2007). Mitochondrial optic neuropathies: how two genomes may kill the same cell type? Biosci. Rep. *27*, 173–184.

Dale, A.M., Fischl, B., and Sereno, M.I. (1999). Cortical surface-based analysis. I:Segmentation and surface reconstruction. Neuroimage *9*, 179–194.

Darian-Smith, C., and Gilbert, C.D. (1994). Axonal sprouting accompanies functional reorganization in adult cat striate cortex. Nature *368*, 737–740.

Engel, S.A., Rumelhart, D.E., Lee, A.T., Glover, G.H., Chichilnisky, E.-J., and Shadlen, M.N. (1994). fMRI of human visual cortex. Nature *369*, 525.

Eysel, U.T. (2009). Adult Cortical Plasticity. In Encyclopedia of Neuroscience, (Oxford: Academic Press), pp. 141–147.

Felleman, D.J., and Van Essen, D.C. (1991). Distributed hierarchical processing in the primate cerebral cortex. Cereb. Cortex *1*, 1–47.

Fischl, B., and Dale, A.M. (2000). Measuring the thickness of the human cerebral cortex from magnetic resonance images. Proc. Natl. Acad. Sci. U.S.A. *97*, 11050–11055.

Fischl, B., Sereno, M.I., and Dale, A.M. (1999). Cortical surface-based analysis. II: Inflation, flattening, and a surface-based coordinate system. Neuroimage *9*, 195–207.

Geuze, E., Westenberg, H.G.M., Heinecke, A., de Kloet, C.S., Goebel, R., and Vermetten, E. (2008). Thinner prefrontal cortex in veterans with posttraumatic stress disorder. Neuroimage *41*, 675–681.

Giannikopoulos, D.V., and Eysel, U.T. (2006). Dynamics and specificity of cortical map reorganization after retinal lesions. Proc. Natl. Acad. Sci. U.S.A. *103*, 10805–10810.

Giedd, J.N., Blumenthal, J., Jeffries, N.O., Castellanos, F.X., Liu, H., Zijdenbos, A., Paus, T., Evans, a C., and Rapoport, J.L. (1999). Brain development during childhood and adolescence: a longitudinal MRI study. Nat. Neurosci. *2*, 861–863.

Goebel, R., Esposito, F., and Formisano, E. (2006). Analysis of functional image analysis contest (FIAC) data with brainvoyager QX: From single-subject to cortically aligned group general linear model analysis and self-organizing group independent component analysis. Hum. Brain Mapp. *27*, 392–401.

Grazina, M.M., Diogo, L.M., Garcia, P.C., Silva, E.D., Garcia, T.D., Robalo, C.B., and Oliveira, C.R. (2007). Atypical presentation of Leber's hereditary optic

neuropathy associated to mtDNA 11778G>A point mutation--A case report. Eur. J. Paediatr. Neurol. *11*, 115–118.

Inglese, M., Rovaris, M., Bianchi, S., Comi, G., and Filippi, M. (2001). Magnetization transfer and diffusion tensor MR imaging of the optic radiations and calcarine cortex from patients with Leber' s hereditary optic neuropathy. J. Neurol. Sci. *188*, 33–36.

Jones, S.E., Buchbinder, B.R., and Aharon, I. (2000). Three-Dimensional Mapping of Cortical Thickness Using Laplace' s Equation. Hum. Brain Mapp. *11*, 12–32.

Kaas, J.H., Collins, C.E., and Chino, Y.M. (2006). Plasticity of Retinotopic Maps in Visual Cortex of Cats and Monkeys After Lesions of the Retina or Primary Visual Cortex. In Plasticity in the Visual System: From Genes to Circuits, R. Pinaud, L.A. Tremere, and P. de Weerd, eds. (New york: Springer), pp. 205–227.

Kaas, J.H., Krubitzer, L. a, Chino, Y.M., Langston, a L., Polley, E.H., and Blair, N. (1990). Reorganization of retinotopic cortical maps in adult mammals after lesions of the retina. Science *248*, 229–231.

Kirkman, M.A., Korsten, A., Leonhardt, M., Dimitriadis, K., De Coo, I.F., Klopstock, T., Griffiths, P.G., Hudson, G., Chinnery, P.F., and Yu-Wai-Man, P. (2009a). Quality of life in patients with leber hereditary optic neuropathy. Invest. Ophthalmol. Vis. Sci. *50*, 3112–3115.

Kirkman, M.A., Yu-Wai-Man, P., Korsten, A., Leonhardt, M., Dimitriadis, K., De Coo, I.F., Klopstock, T., and Chinnery, P.F. (2009b). Gene-environment interactions in Leber hereditary optic neuropathy. Brain *132*, 2317–2326.

Kriegeskorte, N., and Goebel, R. (2001). An efficient algorithm for topologically correct segmentation of the cortical sheet in anatomical MR volumes. Neuroimage *14*, 329–346.

Low, L.K., and Cheng, H.-J. (2006). Axon pruning: an essential step underlying the developmental plasticity of neuronal connections. Philos. Trans. R. Soc. Lond., B, Biol. Sci. *361*, 1531–1544.

Man, P.Y.W., Griffiths, P.G., Brown, D.T., Howell, N., Turnbull, D.M., and Chinnery, P.F. (2003). The epidemiology of Leber hereditary optic neuropathy in the North East of England. Am. J. Hum. Genet. *72*, 333–339.

Mattson, M.P., Gleichmann, M., and Cheng, A. (2008). Mitochondria in neuroplasticity and neurological disorders. Neuron *60*, 748–766.

Newman, N.J., and Biousse, V. (2004). Hereditary optic neuropathies. Eye *18*, 1144–1160.

Salat, D.H., Buckner, R.L., Snyder, A.Z., Greve, D.N., Desikan, R.S.R., Busa, E., Morris, J.C., Dale, A.M., and Fischl, B. (2004). Thinning of the cerebral cortex in aging. Cereb. Cortex *14*, 721–730.

Sereno, M.I., Dale, A.M., Reppas, J.B., Kwong, K.K., Belliveau, J.W., Brady, T.J., Rosen, B.R., and Tootell, R.B.H. (1995). Borders of multiple visual areas in

humans revealed by functional magnetic resonance imaging. Science *268*, 889–893.

Sereno, M.I., McDonald, C.T., and Allman, J.M. (1994). Analysis of retinotopic maps in extrastriate cortex. Cereb. Cortex *4*, 601–620.

Sincich, L.C., and Horton, J.C. (2005). The circuitry of V1 and V2: integration of color, form, and motion. Annu. Rev. Neurosci. *28*, 303–326.

Talairach, J., and Tournoux, P. (1988). Co-planar stereotaxic atlas of the human brain: 3-dimensional proportional system: an approach to cerebral imaging (New York: Thieme Medical Publishers).

Tamnes, C.K., Ostby, Y., Fjell, A.M., Westlye, L.T., Due-Tønnessen, P., and Walhovd, K.B. (2010). Brain maturation in adolescence and young adulthood: regional age-related changes in cortical thickness and white matter volume and microstructure. Cereb. Cortex *20*, 534–548.

Wandell, B.A., and Smirnakis, S.M. (2009). Plasticity and stability of visual field maps in adult primary visual cortex. Nat. Rev. Neurosci. *10*, 873–884.

TABLES AND FIGURES CAPTIONS

Table 1. Demographics and measures of visual acuity and visual field (MD, mean defect; LV, loss of variance) of both left (LE) and right (RE) eyes of LHON carriers. Normal range: MD ±2 dB and a LV < 6 dB^2. Visual dysfunction consistent with subclinical loss is evident.

Table 2. Pearson correlation coefficients computed between visual area thickness and age for controls and LHON carrier groups under and over 21 years old.

Fig. 1. Ocular imaging data of the left eye of a **(left: A,C)** CONTROL, 48 years and **(right: B,D)** a LHON carrier (Table 1, patient 2), 47 years. **(A, B)** Individual OCT neuroretinal thickness maps (color bar codes this measure in µm) centered on the fovea. Relative macula volume/thickness loss can be documented in the inner rings of LHON carrier (total macular volume 6.24 mm^3) comparing to the CONTROL (total macular volume 7.14 mm^3) (see text for group analysis). Imaging data were obtained across a 6 mm circular area centered in the macula. **(C, D)** Sectional retinal scans corresponding to the maps presented on top.

Fig. 2. Occipital inflated (periphery) and flattened (centre) meshes of a LHON patient (Table 1, patient 14). **(A)** Cortical thickness map over the right and left occipital lobes. Due to the high convoluted structure of the cortex we used an automatic algorithm based on the second-order Laplace's equation after the

pre-segmentation of cortical tissues. The output is a pseudo-color map overlaid on 3D meshes for visualization. Using BVQX tools we can export the thickness map of region-of-interest points. **(B,C)** Overlays of retinotopic maps in response to **(B)** Polar Angle stimuli (maps angular position regarding the centre of gaze). The position is represented by a color coded map; and **(C)** Eccentricity representations (maps from posterior to anterior cortex as the stimuli moves from centre (fovea) to periphery of the visual field).

Fig. 3. Functional representation of early visual areas (Table 1, patient 14). **(A)** Polar angle map. **(B)** Eccentricity map. **(C)** Visual field sign map. This technique provides a better approach to delineate the borders of visual areas. It is based on the local gradient (fastest rate of change direction) of each coordinate, polar angle and eccentricity, **(D)** Since adjacent areas alternate with a mirror and nonmirror representation of the visual field, corresponding to the horizontal and vertical meridians, with drawing tools, we can define the early visual areas as regions-of-interest for subsequent analysis.

Fig. 4. Mean cortical thickness is significantly higher in LHON carrier group as compared to the CONTROL group, particularly in extrastriate areas V2 and V3. *p<0.05; **p<0.01. Error bars correspond to 1 SEM.

Fig. 5. Mean cortical thickness of each cortical visual area. Results are from a ROI-based analysis of CONTROL and LHON carrier groups with **(A)** age under 21 years; and **(B)** age over 21 years old. **p<0.01, †p=0.053 *post-hoc* Bonferroni pairwise comparisons. Error bars correspond to 1 SEM.

Fig. 6. Cortical thickness maps over inflated meshes. **(A)** CONTROL, 14 years; **(B)** LHON carrier, 17 years (Table 1, patient 11). For visual inspection a pseudo-color cortical thickness map is overlaid on inflated meshes (dark blue, 0.50mm; light green, 6.00mm). (I, inferior; P, posterior; R, right)

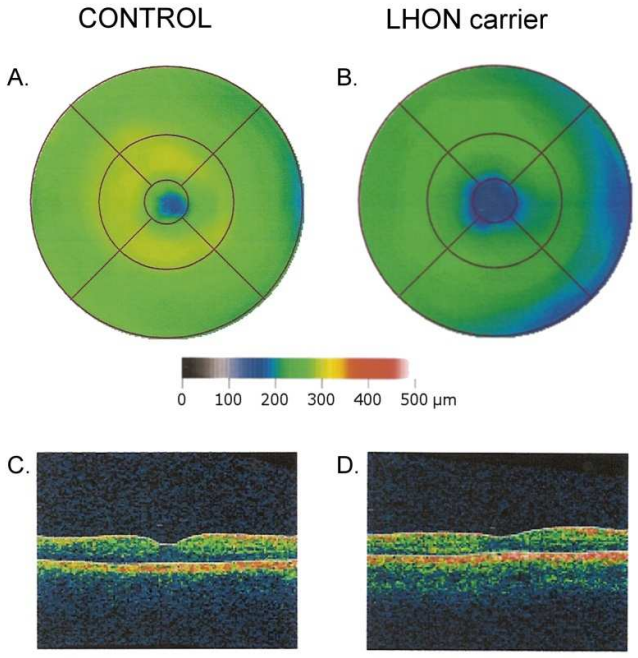

Fig. 1

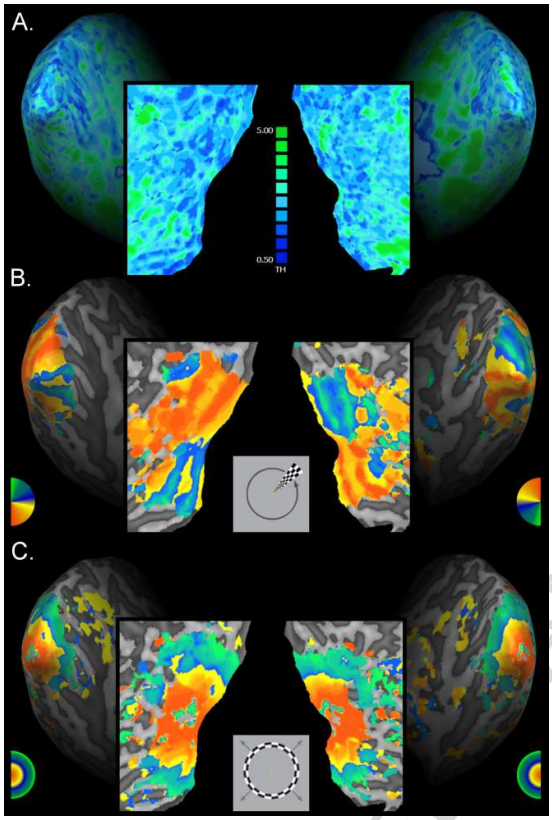

Fig. 2

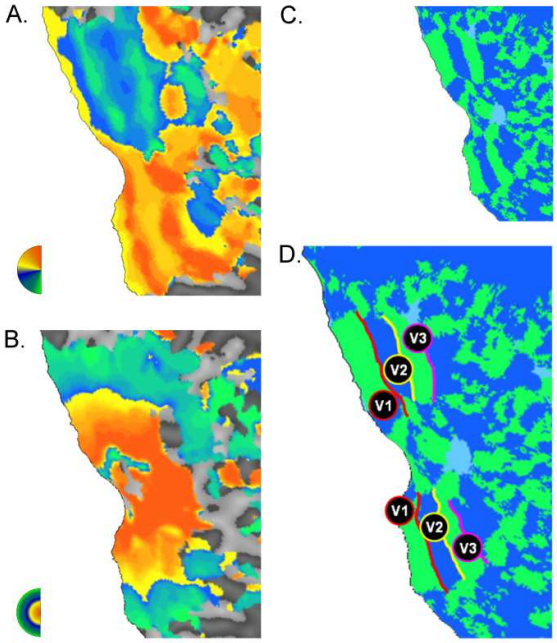

Fig. 3

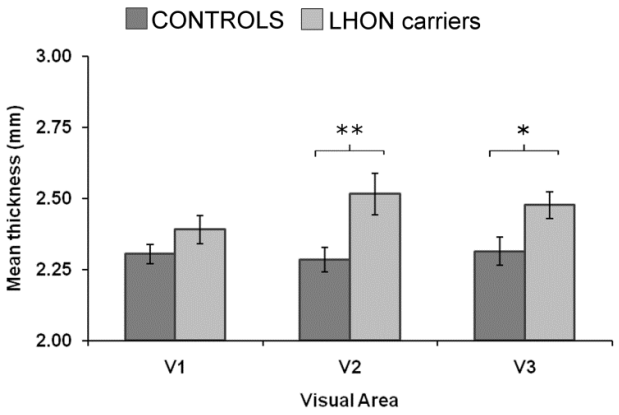

Fig. 4

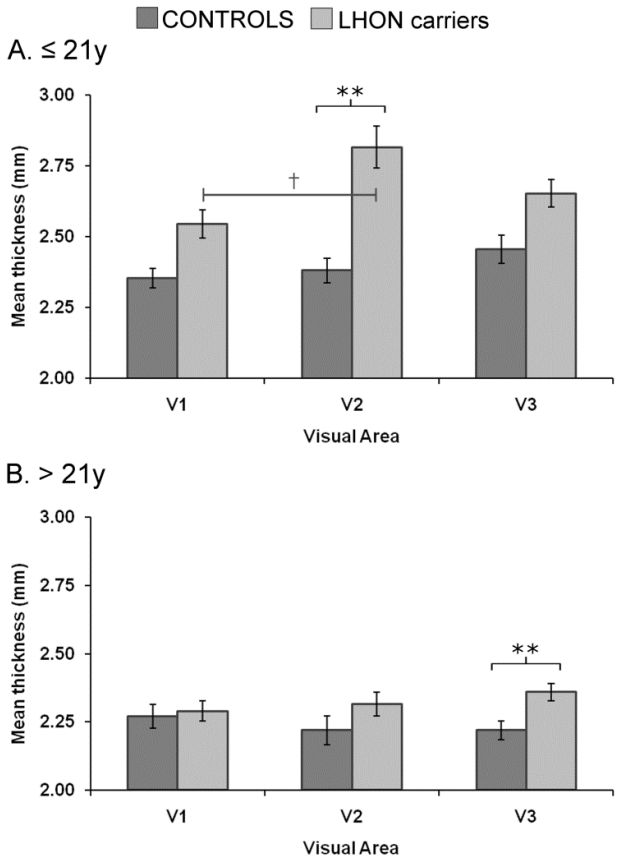

Fig. 5

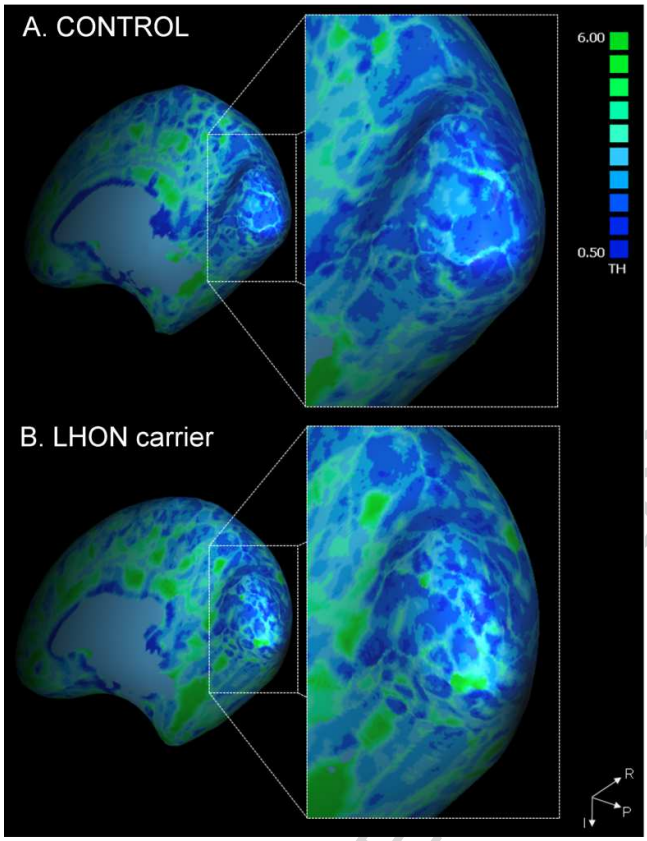

Fig. 6

Table 1

Patient	Gender	Age	Visual Acuity		Visual Field			
					MD (dB)		LV (dB^2)	
		(y)	LE	RE	LE	RE	LE	RE
1	M	47	20/16	20/16	0.7	-0.7	3.3	3.8
2	F	47	20/20	20/20	1.7	1.8	4.4	5.2
3	F	43	20/20	20/20	3.8	2.8	10.3	4.9
4	M	41	20/16	20/16	4.0	4.2	8.3	4.0
5	F	40	20/20	20/20	4.4	4.0	6.6	3.1
6	F	39	20/20	20/20	3.8	5.0	7.9	2.1
7	F	37	20/16	20/16	0.9	1.8	5.1	5.2
8	F	30	20/16	20/16	7.8	7.0	9.1	10.8
9	M	21	20/16	20/16	7.8	5.5	20.4	32.3
10	F	22	20/16	20/16	6.6	3.9	26.7	9.2
11	M	17	20/16	20/16	5.0	3.3	24.1	10.9
12	M	19	20/16	20/20	5.2	2.8	15.2	10.5
13	M	10	20/20	20/20	6.9	4.1	15.7	4.3
14	F	18	20/16	20/16	7.6	7.8	6.7	9.2
15	M	8	20/16	20/20	3.1	3.1	7.9	9.9

Table 2

	CONTROLS				LHON carriers			
	mean thickness (mm)				mean thickness (mm)			
	V1	**V2**	**V3**	**Age** (y)	**V1**	**V2**	**V3**	**Age** (y)
Age ≤ 21y								
V1 mean thickness (mm)	1	n.s.	n.s.	n.s.	1	.688 (.013)	.841 (.001)	n.s.
V2 mean thickness (mm)		1	n.s.	n.s.		1	.763 (.004)	-.857 (<.001)
V3 mean thickness (mm)			1	-.772 (.003)			1	-.833 (.001)
Age (y)				1				1
Age > 21y								
V1 mean thickness (mm)	1	.557 (.016)	.529 (.024)	n.s.	1	n.s.	n.s.	n.s.
V2 mean thickness (mm)		1	.633 (.005)	n.s.		1	n.s.	n.s.
V3 mean thickness (mm)			1	n.s.			1	n.s.
Age (y)				1				1